Improving Nanotribology Performance of Large-Area Metallic Foil Surfaces via Warm Laser Shock-Induced Nanostructure Features

Naveen Kumar Rajendrana[1], Bhawna Wadhwab[2], Awakash Mishrac[3], Dr. Parag Amind[4]

[1]Assistant Professor, Department of Aerospace Engineering, Faculty of Engineering and Technology, JAIN (Deemed-to-be University), Ramanagara District, Karnataka, India, Email Id- r.naveenkumar@jainuniversity.ac.in,
[2]Assistant Professor, Department of Computer Science, Noida Institute of Engineering and Technology, Greater Noida, Uttar Pradesh, India, Email Id- bhawna.wadhwa@niet.co.in
[3]Professor, Maharishi School of Engineering & Technology, Maharishi University of Information Technology, Uttar Pradesh, India, Email Id- awakash.mishra@muit.in
[4]Director, Department of ISME, ATLAS SkillTech University, Mumbai, Maharashtra, India, Email Id- parag.amin@atlasuniversity.edu.in

The restrictions of laser-induced micro forming in nano production mainly stem from surface accuracy and mechanical properties. This study involved the fabrication of nanotechnology line textures on aluminum (Al) foil with a focus on achieving high precision and quality. Additionally, the experimental investigation explored the impact of pulsed laser power and warm laser shock Execution on the production of these lines patterning at the nanoscale. Nano-level line patterning nanotribology was assessed using Atomic Force Microscope (AFS), resulting in the identification of the optimal laser shock imprinting value. This examination explained the improvements in nanotribology performance achieved on large-area metallic foil surfaces through warm laser shock, particularly on Aluminum (Al) foil featuring nanoscale line patterning. The nanotribological characteristics of Nanoscale Line Textured Al Foil (NLTAF) was analyzed using AFS equipped with sharpened probing and colloidal probing made of SiO2. The results of the experiment demonstrated that the use of NLTAF resulted in a reduction of both friction and adhesive force between the AFS probe along with the Al foil. Warm laser shock

imprinting is capable of producing accurate NLTAF with excellent precision. The NLTAF exhibited enhanced the nanotribological properties in comparison to the initial aluminum foil.

Keywords: Atomic Force Microscope (AFS), Pulsed laser power, Warm Laser shock imprinting, nanotribology.

1. Introduction

Metallic foil surfaces are a fascinating demonstration of artistic and industrial innovation, combining beauty and practicality. These surfaces, enriched with a glossy shine, have, beyond their practical beginnings, become an essential component of modern design and other artistic domains (Haifeng et al (2020)). The combination of metallic foils and surfaces is a perfect blend of heritage and contemporary, as these materials have transformed from their simple origins to symbolize luxury, advancement and a deep aesthetic attraction (Haifeng et al (2019)). Metallic foil surfaces reflect individual designs, extending from ancient cultures. Artisans in ancient times, who were aware of the adaptability and reflecting characteristics of metals, conducted experiments to place very thin layers of metallic foils on different surfaces (Mahmood et al (2022)). Starting with ancient Egyptian plating and continuing through the complex silver leaf uses on traditional manuscripts with illumination, those early instances pointed out the lasting popularity of metallic foil surfaces (Li et al(2019)). Throughout the years, this craftsmanship was created, integrating a wide range of materials such as copper, gold, silver and aluminum (Al), each adding its distinct qualities to the overall masterpiece (Stanciu et al (2023)). Metallic foil surfaces had a comeback in the modern era due to technological improvements with new recognition of the interaction between brightness and roughness. Contemporary production processes enable the creation of metallic foils with exceptional clarity and uniformity, empowering architects as well as designers to explore the limits of their creativity (Man et al., (2019)). Metallic decorations can bring an aura of luxury to a space, whereas silver or copper foils add an element of warmth and refinement. Metallic foils include reflecting properties that make them well-suited for compact areas, as they can visually enlarge rooms and increase the interaction of natural light Man et al(2018).

Mathew et al(2021) presented a machine-learning system capable of predicting the Residual strain pattern generated by Laser Shock Peening (LSP). They employed Artificial Neural Networks (ANNs) in a Bayesian approach to construct a reliable forecasting method. The suggested model effectively detected undetected relationships among processing factors and the pattern of enduring stress. Meng et al.,(2019) examined the processing of Ti6Al4V samples using Warm Laser Shock Peening (WLSP) under varying temperatures spanning across 200 and 350 degrees Celsius. Resistance coefficients Unprocessed and WLSP tests were determined using Influence method testing and the enhancement of absorption qualities resulting from WLSP was investigated based on the Microscopic structures in the Ti6Al4V titan metal blend. The findings suggested that vibrating tests experienced large-magnitude shaking pressure on their outer layer. Lu et al(2020) examined the microscopic characteristics of the GH4169 nickel superalloy that had passed the WLSP technique using various laser settings. Observations were conducted of the widespread and entangled

presence of fractures in GH4169 and it was found that the number of dislocations increased following WLSP therapy. WLSP improved the surface hardness and strength of yield by the restructuring of displacements, the promotion of hyper vacancies formation and the establishment of a stable structure with enhanced susceptibility to elevated temperatures, softness and creep. Zhang et al(2021) examined the implementation of warm laser shock imprinting (WLSI) tests and the subsequent research on elevated temperature recovery. The method of numerical modeling was employed to evaluate the strain and stress distributions. Subsequently, the laser-affected samples' surface structure and physical attributes were examined and assessed using a 3D visual profile and a "scanning electron microscope (SEM)." Finally, the study showed that the WLSI technique improved the thermal resistance of metals' 3D microstructures and outperformed laser shock imprinting (LSI) by obtaining more height and quality during the formation process.

Li et et al(2022) proposed a novel approach named Micro-Laser Shock Peening (Micro-LSP) for enhancing the outside properties and durability of AISI 9310 steel by LSP. The studies were conducted to examine the effect of pulses varying in energy (50,150,200 megajoules) on surface structure, mechanic features and wearing behavior. The results indicated an elevated level of surface irregularity and an appearance of minor crises, which affected the overall shape and structure. Somasundaram et al(2023) utilized microscopy with optical fibers to examine the microstructure in the EV31A metal. Furthermore, a "field emission scanning electron microscope (FE-SEM) with Energy Dispersive Spectroscopy (EDS)" evaluation was utilized to examine the structure of wear and "X-Ray Diffraction (XRD)" evaluation was conducted prior to and after the examination for wear. The tribological characteristics were predicted by employing a ternary-layered ANN and a fine Gaussian Support Vector Machine (SVM) that had been optimized for the task. The ANN model displayed a robust association with the experimental findings, demonstrating efficacy in forecasting tribological behavior.

Cavaleri et al(2019) examined the creation of a dependable and resilient ANN with the ability to forecast the tribological characteristics of three extensively alloyed tool steel types. The Backpropagation Neural Network (BPNN) model provided significant results, demonstrating that nitrocarburizing surface treatment improved resistance to wear, higher bulk roughness prolonged steady-state wear and operating variables impacted the choice of steel grade. Maleki et al(2023)investigated the impact of LSP treatment on various aspects of "laser powder bed fused (L-PBF) AlSi10Mg tests". The study emphasized the effects of various laser pulse overlapping and energy. LSP induced strain deformation on the outer layer, which increased further with the intensity of the laser beam. The results showed that increasing both pulsing overlapping and energy could enhance the hardness of the surface and corrosion resistant steel (CRS), with pulsing frequency having greater effects.

The aim of this study is to enhance nanotribology (NT) performance on large-area metallic foil surfaces through warm laser shock, creating nanostructure features. The remaining segments of the study were classified into the following categories: The methodology is discussed in section 2. Section 3 includes results and conclusion in section 4.

2. Methodology

2.1 Experimental setup

WLSI tests use a 1 KHz Q-switched Nd: YAG laser (Laser System XYZ-10, produced by Photonics Industries, India) having a pulse length of 10 ns, 20 μm beam thickness and 355 nm intensity. Figure 1 shows the nanoscale LSI design. In Figure 1(a), the specimen, absorbent level and restricting coating are put on a mold and set on an even table. The test surface for LSI was a 13 μm thickness standard Aluminum Foil (AF). The restricting layer is 2 mm thick K9 glass, whereas the absorption coating is 13 μm wide black AF. The holder compresses every layer to prevent clearance between constraining and absorbent levels from diminishing the laser shock Plasma outburst. Figure 1(b) and (c) exhibited LSI nanoscale texture 3D schematics. Laser shock molds metal foil and creates textures on its surface. The study introduces a warm laser shock procedure that places AF straight on an even table Figure 1(a), Warm laser shock without the use of a Nanoscale Wafer Mold (NWM) waves compress rough metal foil on a smooth table. All warm laser-shocked AF is shocked with 100 μJ energy from a pulsed laser and a 0% ratio of overlap.

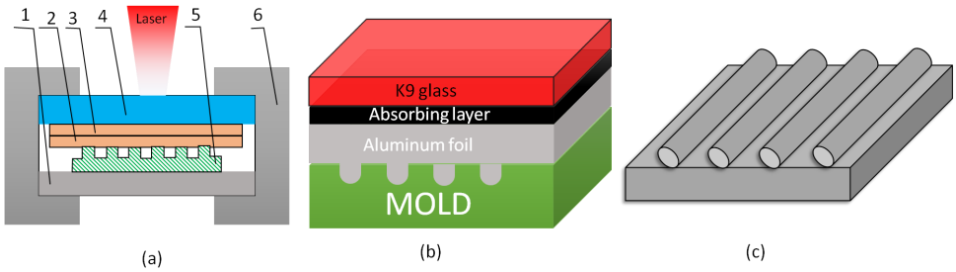

Figure 1(a) WLSI texture Procedure 1. Smooth table, 2. Sample, 3. Absorbing layer, 4. Confining layer, 5. NWM, 6. Holder, (b) Three-dimensional representation of WLSI, (c) nanoscale texture created through imprinting

(Source: author)

AFS images of the initial AF and mold are shown in Figure 2. The Initial AF area was uneven and rough. Silicon wafers with a depth of 10x10 mm area were used to create the nanoscale mold with periodic lines. In Figure 2, the nanoscale wafer molding zone shape curve indicates a 1 μm line texture time and a 500 μm grooved width. Every experimental AF, mold and K9 glass is sanitized in acetone for five minutes. The warm laser mark program controls the pace and position of the pulsed ultraviolet laser system on a Galvo-driven scanning system for computers. The scanning with laser velocity and line density in the laser printing program is used to get the LSI overlapping ratio. The study presents a warm laser shock procedure and places the AF straight on an even table (Figure 1(a)) without microscopic dimensions wafers molding for laser shock. Warm laser shock wave flattens rough AF on a smooth table. All warm laser-shocked AF undergoes shock with 100 μJ pulsed laser power and 0% delay rate.

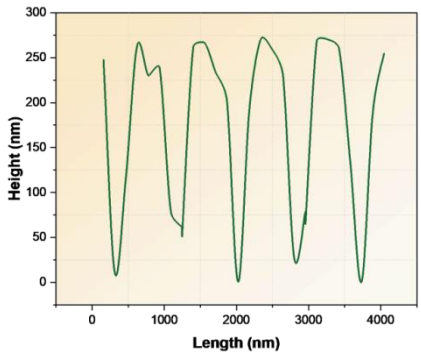

Figure 2NWM cross-section profile curve

(Source: author)

An AFS (XYZ-2000, NanoPro Analyzer, India) combined with "Leica optical microscope (LOM)" analyze collection and molding shape. A Berkovich diamond-equipped Nano-indenter G200 from Keysight indentation measures LSI AF the nanoindentation roughness. Warm laser-imprinted components are tested for micro-tensile characteristics using the Chixi MTS-4500. An electrolytic test is done at ambient temperature. Electrochemical tests require 3.5% NaCl. open circuit potential (OCP), electrochemical impedance spectroscopy (EIS) and Potentiodynamic polarization (PDP) are evaluated utilizing a standard platinum foil in a three-electrode configuration as the neutral electric terminal and a silver chloride half-cell as the stable electrode on the CHI660D electrical workstation to study materials erosion.

Evaluation of adhesion and resistance forces on nanostructured surfaces with textures using commercialized AFS utilizing a pointed probe and SiO2 Microgel probe (10 microns radius, 0.3 N/m elastic constant, 13 KHz resonant frequency). LSI technique ablates absorbed layer AF with a laser beam and vaporizes it to cause plasma explosions. The pulse of the warm laser-generated brief, intense pressure zone vibrations propagated to the AF and ultra-small wafer molded contact at multiple GPa. After deformation from plastic, the AF creates nanoscale surface texture. Deformation due to plasticity happens at the pinnacle of pressure spread of shock waves induced by warm lasers and it surpasses the "Hugoniot Elastic Limit (HEL)." The following equation describes the link between HEL and dynamic yielding strength:

$$\mathrm{HEL} = \frac{1-u}{1-2u2}\sigma_z^{dzm} \quad (1)$$

u is the ratio of Poisson. Distribution of pressure and transmission of warm laser-induced waves of shock. Based on the laser's energy thickness, a shock wave's pressure at its peak can be calculated. A shock wave pressure peak equation is:

$$O_{max} = 0.01\sqrt{\frac{\alpha}{2\alpha+3}} \times \sqrt{\frac{2Y_1Y_2}{Y_1+Y_3}} \times \sqrt{J_0} \quad (2)$$

where the target substance has shock impedance Y1 (Y1 = 1.5 × 〖10〗^6 〖gcm〗^(-2) •s^(-1))and K9 glasses has shocking impedance Y2 (1.14 × 106 〖gcm〗^(-2) •s^(-1)). The transformation proportion of the fusion materials connection (α) is fixed at 0.1. The laser's

intensity (I_0)and pulsed energy (E) are related by the equation:

$$J_0 = \frac{4F}{\pi\tau C^2} \quad (3)$$

F Represents pulsed energy from the warm laser, with C (20 μm) and τ (10 ns) representing the beam's diameter as well as pulse time.

3. Result and Discussion

3.1 The nanotribology frictional characteristics of aluminum foil with nanotribology line texturing (NSLT)

Numerous experts generated different patterns on substances using various methods to study Tribological Properties (TP) and surface NSLT technologies improved the wear and friction of friction groups. The article evaluated the NT behaviors of NSLT foil made of Al using sharper probes, colloid probes and AFS interaction methods. The AFS's more robust probes were used to study surface NT attributes due to their high quality and inexpensive cost. The point diameter was tens of nanometers. tribology for AFS sharper probe was shown in Figure 3 (a). TP of single-line roughness was measured using the short probes. The leading edge diameter was 30 nm and the cantilever had 0.2 (Newtons per Meter elasticity) constants and 13 (Kilohertz) resonance frequency. Because the AFS sharper probe point diameter was lower than the molded grooves' width, the micro-level TP of NSLT was unable to be measured. In Figure 3 (b), a mercantile AFS particle instrument was used to analyze the TP of “Nano Line Textured Aluminum Foil (NLTAF)." A 10 μm SiO2 colloid sphere was suspended to the probed cantilever. AFS probe scanning directions conceptual on NSLT are shown in Figure 3 (c).

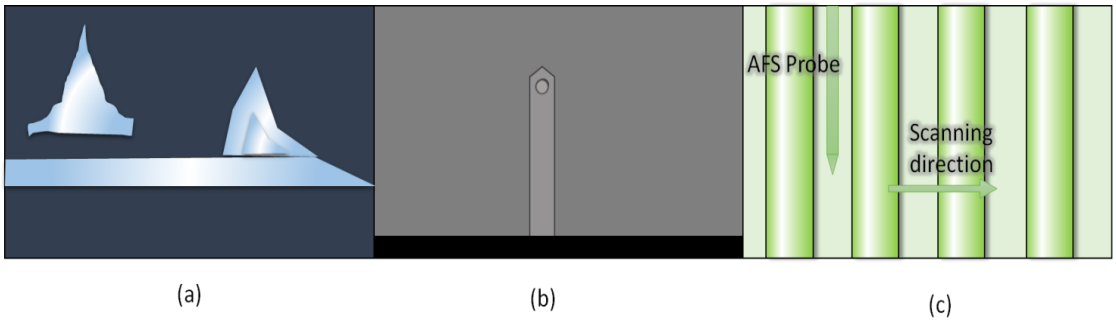

Figure 3(a) The AFS acute probe; (b) the AFS particulate probe; (c) The schematic illustrating the scan orientation of a nanoscale line-textured AFS sharp probe.

(Source: author)

Figure 4 (a) shows the resistance force loading curve of NSLT on "Warm Laser-Shocked Aluminum (WLSA)". AFS measures the foil's sharper probes with an average workload limit of 0 V to 2.5 V. The initial foil of the Al surface had the most friction below the typical load. The elevated frictional resistance with standard load and Friction force-load characteristic slopes mirrored the coefficient of friction for the surface. NLTAF and WLSA have fewer

friction forces than the original AF at the same typical load. When the AFS sharper probes were used to assess nano friction, the AF nano line roughness decreased friction. The Load-dependent frictional force plot slope was the AF frictional ratio, determined by matching every sample's friction loading curves in Figure 4 (a). In Figure 4 (b), conventional and NLTAF coefficients of friction were displayed. Warm Laser shock reduced AF from 0.28 to 0.13. NLTAF has less friction than the original AF. As pulsed laser energy rose, the NLTAF friction coefficient was raised.

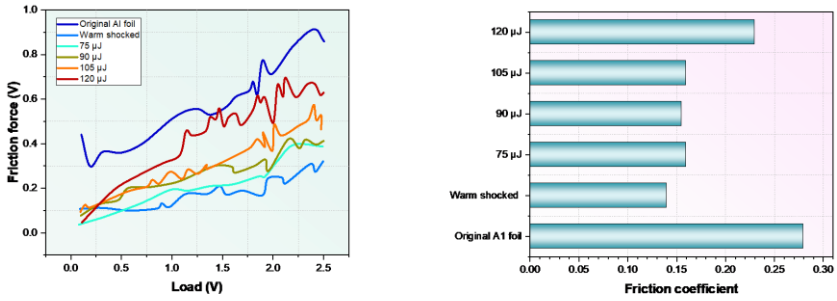

Figure 4(a) Friction force-load curves for NLTAF under varying laser energy conditions; (b) The friction coefficients associated with NLTAF

(Source: author)

The friction looping curves of NLTAF were determined through the AFS sharper probe (Figure 5). AFS defined friction force as the distinction between tracing and retracing friction pressure lines. Figure 5 shows the friction looping curve of NLTAF created using 120 µJ pulsed laser shocks imprint. It observed periodic changes in the force of friction on the friction loop curves. The frictional force varies between 0.05 volts and 0.3 volts during 120 µJ, WLSI. The LSI consistent nano line patterns on pre-irradiated foil metal periodic the force of friction changes.

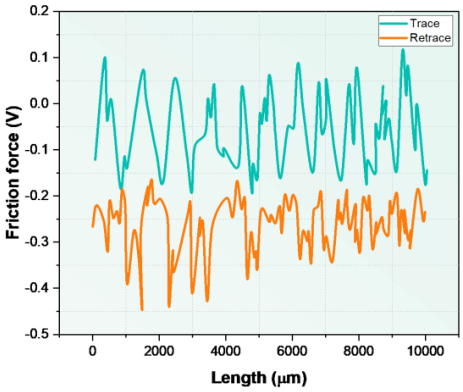

(6)

Figure 5The friction loop curve for NLTAF using laser pulse energy of 120 µJ.

(Source: author)

Figure 6 (a) AFS colloid probe adhesion curves for standard foil Al and WLSA were shown in (b). WLSA (1.18 V) has a lower force to adhere than the original Al sheet (1.73 V). Figure. 6 (c) shows NLTAF Adhesion forces with different puls intensities.LSI reduced WLSA adhesiveness. The adhesive strength of NLTAF increases with LSI pulse strength.

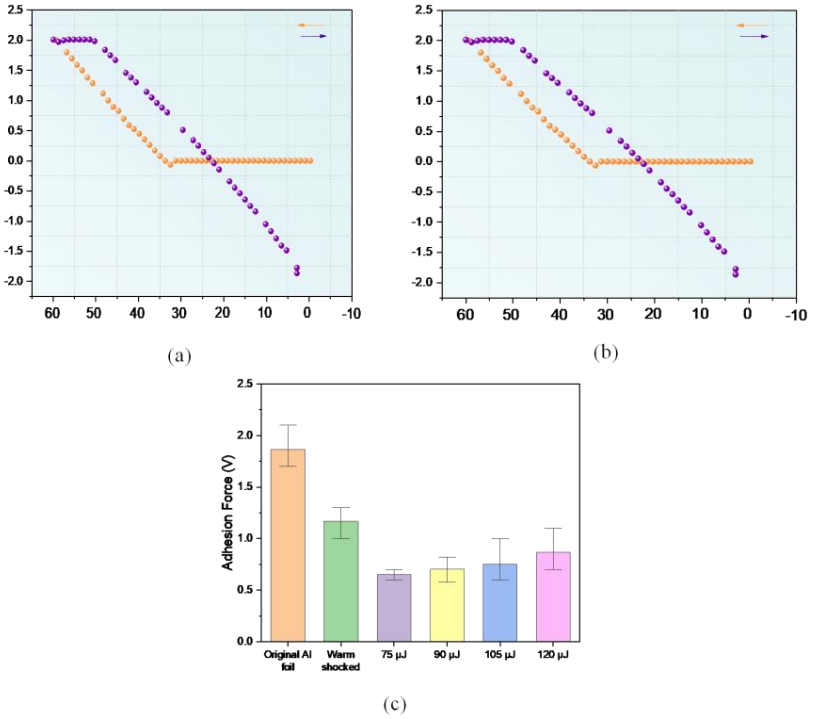

Figure 6(a) The "adhesive force curve" of initial AF evaluated by AFS particle analysis device;

(b) "Adhesive force curve" of warm laser-pulsed AF evaluated by AFS particle analysis device;

(c) "Adhesive force" of NLTAF with different pulse laser energies.

(Source: author)

Figure 7(a) showed AFS colloid probe-detected NLTAF frictional force-load curves. According to the study, the conventional foil of Al had the highest force of friction under a typical load, but warm laser shock reduced it. NLTAF had less friction than traditional and WLSA. Increased laser pulsed energy reduced friction on NLTAF under average load. The NLTAF has very little friction at 120 Mj, LSI power. Colloid probes and NS line roughness coefficients of friction were calculated from the slope of the frictional force-load curves, which were linear. LSI Figure 7 (b) depicted friction coefficients for aluminum foil. NS original friction coefficients AF and WLSA were 0.68 and 0.47. NLTAF had less friction than the original and WLSA with increased energy from a pulsed laser. The NS straight-line pattern on AF deepened and the coefficient of friction was reduced. NSLT reduced aluminum foil-AFS nanoparticle probe friction.

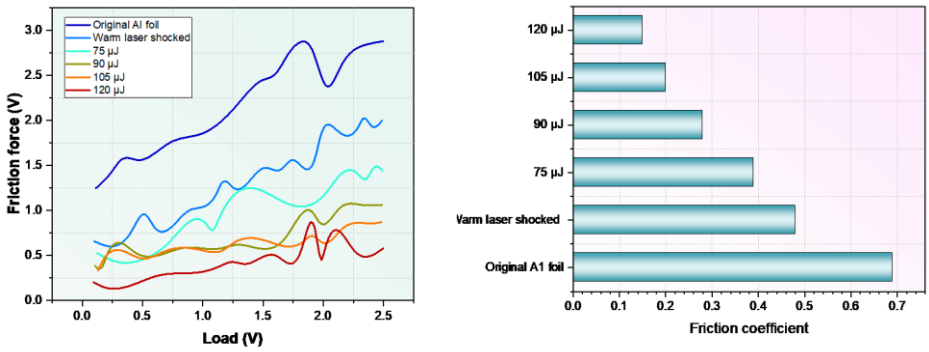

(a) (b)

Figure 7(a) Friction force-load profiles of NLTAF evaluated by AFS particulate probe; (b) the friction values of NLTAF

(Source: author)

The bonding strength among materials in NS was mostly London forces, Capillary vessels and molecular adsorption. The study could neglect chemical bonds, adsorption and electric forces owing to the AFS alloy probing wrap in the air. AFS probe-NSLT friction was caused by capillary forces and intermolecular bonds. The adhesion force calculation is:

$$E_{ad} = E_D + E_{ucx} \quad (4)$$

Here E_adare adhesives, E_D is a capillary vessel and E_ucx is London dispersion forces. Close surfaces of contact create a thin water layer among particles in humid environments. Water film produced a liquid bridge and caused two items to stick together, creating a capillary effect. The Spherule-plane interaction model in Figure 8 describes the adhesive pressure among the AFS probe and AF. The practical estimation for the water film thickness on AF is:

$$g = 0.3(Q_g) + 0.5f^{20(Q_g-1)} \quad (5)$$

Where Q_g is the moisture level. In accordance with the Kelvin and Laplace formula, we can evaluate capillary bonding E_d:

$$E_d = \frac{\gamma_{ln}}{\gamma_l} B_n = \frac{Q_h S ln(Q_g)}{U_0} B_n \quad (6)$$

Where Q_h is universal gas constant; S is atmospheric temperature; U_0is water molar volume and B_n is the Connection region.

$$B_n = \pi(Q \sin \phi)^2 \quad (7)$$

The London force E_{vdw}can be represented as:

$$E_{vdw} = \frac{GQ}{6b^2} \quad (8)$$

Where G is the power punch persistent and b is the separation between the contact surfaces of two solid objects. Hence, the formula (9) represents the force of adhesion among the AFS

detector tip and AF.

$$E_{bc} = \frac{Q_h S \ln(Q_g)}{U_0} B_n + \frac{GQ}{6b^2} \quad (9)$$

It found that the area of contact B_n determined the adhesive pressure among AFS probing tip and AF at a fixed temperature. AFS colloid probing tip diameter decided the area of contact B_n.

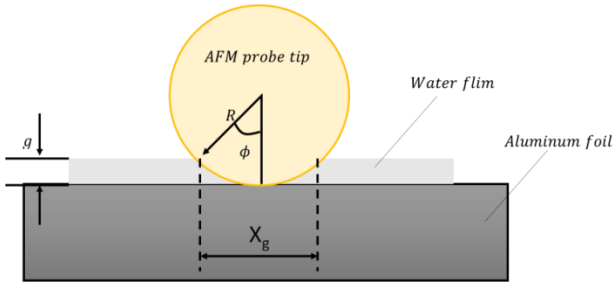

Figure 8The "capillary force" among the AFS point and AF

(Source: author)

The ragged bands, flaws and microscopic fracture on the initial AF impaled the water-based film and touched a colloidal sphere when the AFS colloid probing touched them, creating an intense adhesion force. Formula (9) indicates that the area of the B_n determines the adhesive strength E_bc. Due to the warm laser's shocked AF's flat surface, the AFS colloid probe's area of contact B_n was enormous as it touched the WLSA, creating a high adhesion force. Figure 9 depicts the AFS colloidal probe-NSLT contact model. The consistent NSLT on AF blocks water film at the interaction interface and reduces contact area B_n. NLTAF reduced adhesion compared to WLSA. The depth and shape of the NSLT on WLSA varied with LSI pulsed power, while the duration was fixed and the highest feature curvature was circular. NSLT thickness increases with warm laser-pulsed energy. During the interaction, a colloidal probe and texture had a smaller contact area, decreasing adhesive strength. When the LSI energy of the warm laser pulse was substantial, the NSLT with increased depth and a more pronounced sharpness on the top can reduce cohesion strength.

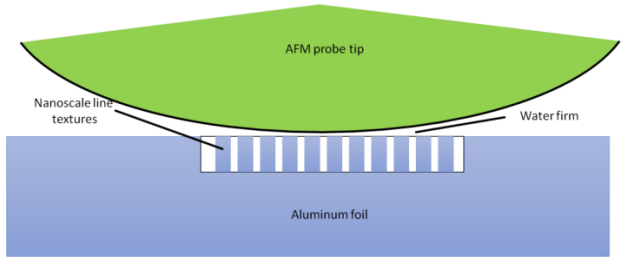

Figure 9"Sphere-plane contact model" among AFS probe and NLTAF.

(Source: Author)

When measuring the NSLT force of friction with the AFS sharp probe, the lateral force was the frictional force across the probe point and AF. The frictional pair interaction models were

sole peaked connection at tribological characteristics over the probe tip and materials surface tribology dominated friction behavior. The frictional force affected the morphological profile curve and slope. AFS's sharper probing point size was 30 nm and NSLT groove's width on AF was 500 nm. The connection between AFS more robust probes and NSLT texturing is a single-peaked connection, as shown by the ratchet model in Figure. 10

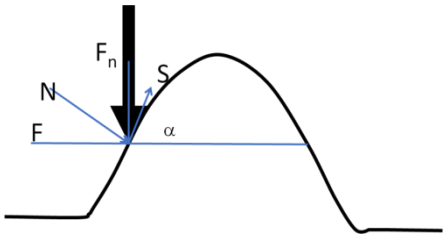

Figure 10Ratchet model

(Source: author)

The AFS sharper probe-NSLT pressure diagram is shown in Figure 10. Bending on the AFS pointed probed tip was a lateral force F. The forces balancing formulae when the sharp AFS probe shifted horizontally on NSLT were:

$$M = E_m \cos\alpha + E \sin\alpha \quad (10)$$

$$T = E \cos\alpha - E_m \sin\alpha \quad (11)$$

Combined the equations (10) and (11):

$$E = \frac{M \sin\alpha + T \cos\alpha}{M \cos\alpha - T \sin\alpha} E_m = \frac{\tan\alpha + \mu_0}{1 - \mu_0 \tan\alpha} E_m \quad (12)$$

The study found that lateral force F is influenced by average load Fn and morphological profile curved slopes (tanα). The friction force increases with the ramp of morphological outline curves when the standard load Fn remains immutable.

Figure 11 (a) shows the NSLT profiling plot and its differential to study the force of friction in the F-tribology profiles' curved connection. NSLT profile curve derivatives are modified like a profile curve. NSLT force of the friction curve and profile derivative are shown in Figure 11 (b). The frictional resistance curve resembled the NSLT derivatives curve. The AFS sharp probe tip-NSLT friction model matched the ratchet model. The friction force was linked to tanα and its modification was linked to the NSLT pattern slope.

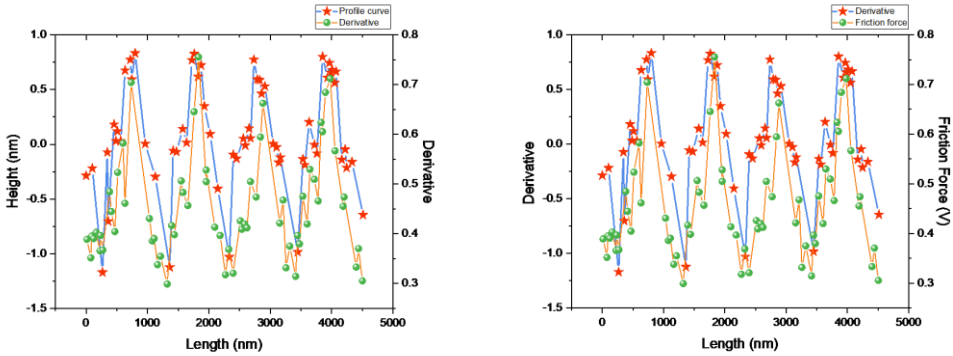

Figure 11(a) Outline curve and NSLT derivatives on heated laser-shrunkAl; (b) the derivation of NSLT profiling and frictional resistance curve.

(Source: author)

Warm laser shock-imprinted NSLT was distributed on AF and had symmetric profiles. The formula for symmetric profile mean

force of friction was:

$$E = \frac{1}{2}\left(\frac{\mu_0 - \tan\alpha}{1-\mu_0\tan\alpha} + \frac{\mu_0 - \tan\alpha}{1-\mu_0\tan\alpha}\right)E_m = \left(\frac{1+\mu_0^2}{1=\mu_0^2\tan^2\alpha} - 1\right)E_m \quad (13)$$

According to Equation (13), the frictional strength of an individual peak is influenced by tanα, while the standard load E_m remains constant. The mean force of friction rises with the NSLT design slope. When α = 0, AFS sharper probe and AF exhibited smoother plane friction, with WLSA force of friction lower than NLTAF. The AFS sharp probe friction force was expected if the NSLT profile slope was downward under a constant texture period. Since NSLT was less than the SiO2 colloid probe, the interaction models among the AFS nanoparticle probe and NSLT were surfaces sliding while measuring frictional force.

$$E = \pi B = \pi\tau b^2 \quad 14)$$

τ represents material shear stress and an indicates the connection distance among the AFS nanoparticle probe interacting with the material surface.

Figure 12 showed the AFS colloid probe-NSLT contact type design. The thick stripes decreased the contact surface between the colloid probe and the original metal, as seen in Figure 12 (a). Yet, shifting roughness striping would impede AFS colloid probe mobility. The colloid probe cantilever provided greater input volt indication, detecting the maximal force of friction on initial AF. Compared with the warm laser WLSA, the NSLT decreased the surface area between AFS particle probe and AF, reducing NLTAF friction. With increased warm laser intensity, NSLT depth on AF and top profile curve raised. The steep top profile of NSLT minimized the area of contact between the AFS nanoparticle tip, reducing friction. It revealed that NSLT reduced AF friction.

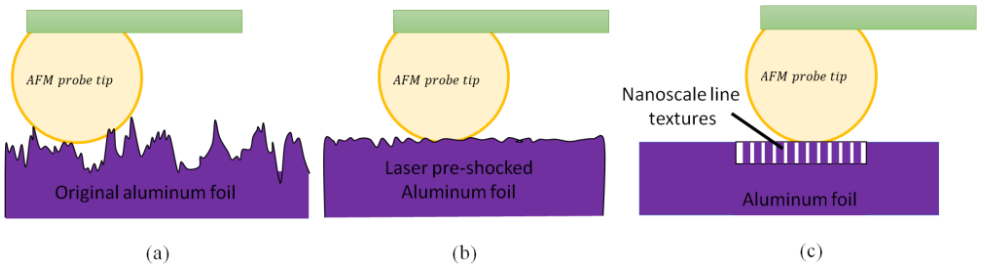

Figure 12The Contact model representation among AFS colloidal probe and AF: (a) Connection with initial Al foil; (b) Connection with warm laser shock AF; (c) connection with NLTAF.

(Source: author)

4. Conclusion

This study introduces a warm laser shock method to enhance the NT Performance of AF, Top-notch nanoscale line patterns with varied successfully achieved depths were created on AF. Through hypothetical research and experimentation, researchers examined the mechanical features and performance of the nanotribological and frictional movement of NLTAF. Significant findings emerged. Using LSI, nanoscale line patterns over a large area patterns were created on AF, resulting in enhanced NT following warm laser shock. Textural patterns at the nanoscale were accurately and uniformly embossed on warm metal foil subjected to laser-induced shock. The depth of Nano-level line patterns can be adjusted by modifying pulse laser energy. LSI enhanced the nanoindentation toughness of textured at the NLTAF, with a hardness of 0.35GPa at 120 μJ energy from laser pulses compared to the initial AF. LSI increased AF tensile and yield strength but decreased ductility. The better nanotribological performance was achieved with NLTAF. The comprehensive characteristics of molded Al foil were enhanced by refining the grains and twining the dislocations to generate solid fault zones. Tiny line features modify AFS probe-aluminum foil adhesion and friction. The Microscale line surface characteristics adjusted the frictional resistance among the AFM microprobe and fine-grained line textures. Microscale line pattern friction was related to the outline curve slope. It shows that microscale line pattern diminish clinging and shearing when an AFM particle probe contacts AF.

References

1. Cavaleri L, Asteris PG, Psyllaki P.P, Douvika M.G, Skentou A.D, Vaxevanidis N.M. (2019) Prediction of surface treatment effects on the tribological performance of tool steels using artificial neural networks. Applied Sciences, 9(14), p.2788.DOI: 10.3390/app9142788
2. Haifeng Y, Fei X, Kun L, Jiaxiang M, Haoxue C, Hao L, Jingbin H (2019). Research on temperature-assisted laser shock imprinting and forming stability. Optics and Lasers in Engineering, 114, 95-103. DOI: 10.1016/j.optlaseng.2018.11.002
3. Haifeng Y, Le, J, Kun, L, Yan, W, Fei, X, Hao L, Jingbin, H(2020). High precision complete forming process of metal microstructure induced by laser shock imprinting. The International Journal of Advanced Manufacturing Technology, 108, 143-155. DOI: 10.1007/s00170-020-05415-6

4. Li X, Wang X, Shen Z, Ma Y, Liu H (2019). An experimental study on micro-shear clinching of metal foils by laser shock. Materials, 12(9), 1422. DOI: 10.3390/met12010077.
5. Li X, Zhou L, Zhao T, Pan X, Liu P. (2022). Research on Wear Resistance of AISI 9310 Steel with Micro-Laser Shock Peening. Metals, 12(12), 2157. DOI: 10.3390/met12122157.
6. Lu Y, Yang Y, Zhao J, Yang Y, Qiao H, Hu X, Wu J, Sun B. (2020). Impact on mechanical properties and microstructural response of nickel-based superalloy GH4169 subjected to warm laser shock peening. Materials, 13(22), p.5172. DOI: 10.3390/ma13225172
7. Mahmood M. A, Chioibasu D, Ur Rehman A, Mihai S, Popesc A.C (2022). Post-processing techniques to enhance the quality of metallic parts produced by additive manufacturing. Metals, 12(1), 77. DOI: 10.3390/met12010077
8. Maleki E, Unal O, Shao S, Shamsaei N. (2023). Effects of Laser Shock Peening on Corrosion Resistance of Additive Manufactured AlSi10Mg. Coatings, 13(5), 874.DOI: 10.3390/coatings13050874
9. Man J, Yang H, Liu H, Liu K, Song H (2018). The research of micro pattern transferring on metallic foil via micro-energy ultraviolet pulse laser shock. Optics & Laser Technology, 107, 228-238. DOI: 10.1016/j.optlastec.2018.05.046
10. Man J, Yang H, Wang Y, Chen H, Xiong F (2019). Study on controllable surface morphology of the micro-pattern fabricated on metallic foil by laser shock imprinting. Optics & Laser Technology, 119, 105669. DOI: 10.1016/j.optlastec.2019.105669
11. Mathew J, Kshirsagar R, Zabeen S, Smyth N, Kanarachos S, Langer K. Fitzpatrick M.E (2021). Machine Learning-Based Prediction and Optimisation System for Laser Shock Peening. Applied Sciences, 11(7), p.2888. DOI: 10.3390/app11072888.
12. Meng X, Zhao Y, Lu J, Huang S, Zhou J, Su C. (2019). Improvement of damping property and its effects on the vibration fatigue in Ti6Al4V titanium alloy treated by warm laser shock peening. Metals, 9(7), 746. DOI: 10.3390/met9070746
13. Somasundaram M, NarendraKumar U, Annamalai A.R, and Muthuchamy A. (2023) High-temperature tribological performance of stir-cast and heat-treated EV31A magnesium alloy: Experiments and predictions. Heliyon, 9(8).DOI: 10.1016/j.heliyon.2023.e19055
14. Stanciu E.M, Pascu A, Croitoru C, Roată I.C, Cristea D, Tierean M.H, Hulka I, Petre I.M. and Mirza Rosca, J.C. (2023) Functional Surfaces via Laser Processing in Nickel Acetate Solution. Materials, 16(8), p.3087. DOI: 10.3390/ma16083087
15. Zhang B, Yang H, Xiong F, Liu H, Hao J, Liu X. (2021) Research on the transient forming process and high-temperature stability mechanism of warm laser shock imprinting. Optics and Lasers in Engineering, 146, p.106719. DOI: 10.1016/j.optlaseng.2021.106719